Available online at www.sciencedirect.com
ScienceDirect
International Journal of Mass Spectrometry 266 (2007) 97–113
International Journal of Mass Spectrometry
www.elsevier.com/locate/ijms

Mass spectrometric characterization of small oxocarboxylic acids and gas phase ion fragmentation mechanisms studied by electrospray triple quadrupole-MS/MS-TOF system and DFT theory

B. Kanawati *, S. Joniec, R. Winterhalter, G.K. Moortgat

Max-Planck Institute for Chemistry, Atmospheric Chemistry Division, P.O. Box 3060, D-55020 Mainz, Germany

Received 4 May 2007; received in revised form 21 July 2007; accepted 21 July 2007
Available online 28 July 2007

Dedicated to Prof. Dr. Karl-Peter Wanczek for his 67th birthday.

Abstract

Monocarboxylic acids with acyl functional group such as 5-oxohexanoic acid and 6-oxoheptanoic acid were characterized experimentally by electrospray ionization coupled to a triple quadrupole and TOF analyzer hybrid system. Collision-induced dissociation experiments at different activation energies were done to elucidate possible fragmentation pathways. These pathways were also studied on the theoretical level using DFT B3LYP/6-311++G(3df,3pd)//B3LYP/6-31+G(d) + ZPVE calculations. While all monocarboxylic acids fragment under loss of CO_2 and H_2O starting from their parent anion $[M-H]^-$, an unusual fragmentation behaviour could be observed in case of 5-oxohexanoic acid. Synchronous CO_2 and CH_2CH_2 elimination in a concerted mechanism was responsible for the lack of $[M-H–CO_2]^-$ fragment ion. New anionic gas phase cyclization processes could be discerned in case of 5-oxohexanoic acid. Mechanistic differences in the fragmentation pathways of $[M-H]^-$ anions formed from 5-oxohexanoic acid and 6-oxoheptanoic acid after deprotonation were investigated both experimentally and through DFT calculations. Successive water, ketene CH_2=C=O, and H_2 eliminations were observed in the CID spectra of 6-oxoheptanoic acid parent anion. CO_2 ejection from the parent ion of 6-oxoheptanoic acid was inhibited due to the lack of stabilization for the formed fragment ion.

Keywords: Oxocarboxylic acid; DFT; CID; Q-TOF; Fragmentation mechanism

1. Introduction

Dicarboxylic acids and ketocarboxylic acids [1] are of great importance in the atmospheric and marine sciences. Many organic compounds, which belong to these two categories were successfully identified in ice core samples [2,3], in the oceanic atmosphere [4], urban aerosols [5–8] and in organic aerosols produced as a result of monoterpene ozonolysis [9]. Carboxylic acids and their keto analogues could be even identified in human plasma [10] and urine [11].

Negative ion mass spectrometry allowed to generate ions of many important species [12], whose fragmentation behaviour delivered useful information [13] for structural elucidations. Combined with experiments in the positive ion mode and collision-induced dissociations of cationic organic compounds, the accuracy of the structural determination can be further enhanced. The importance of negative ionization began with the advent of chemical ionization. Studies in the negative ionization mode were continued with fast atom bombardment [14] (FAB) technique and were recently intensified upon the development [15] of electrospray [16] and atmospheric pressure chemical ionization (APCI) sources [17,18].

Water and carbon dioxide eliminations were observed from the $[M-H]^-$ parent ions of mono- and dicarboxylic acids as a result of low energy collisional fragmentation event. Grossert et al. [19] have shown that carbon dioxide elimination takes place from the non-ionized carboxylic group of the investigated dicarboxylic acids. The mechanism of water loss from a monocarboxylic acid had not been completely understood, until Jensen et al. [20] showed that the following reaction takes place (Eq. (1)).

* Corresponding author. Tel.: +49 6131 305497.
E-mail addresses: kanawati@t-online.de, Kanawati.B@gmail.com (B. Kanawati).

1387-3806/$ – see front matter © 2007 Elsevier B.V. All rights reserved.
doi:10.1016/j.ijms.2007.07.014

Once formed, the ion-neutral complex between DO^- anion and the neutral ketene can dissociate through deuterium abstraction from the ketene by OD^- anion releasing D_2O and thus generating a ketene anion, which can be well stabilized through electronic delocalization. Gas phase ion-neutral complex formation and unimolecular dissociation are extensively discussed in the literature [21–24].

Deuterium experiments are not always helpful in deciphering gas phase reaction mechanisms, especially in cases, where collisionally activated ion dissociations take place. This is due to the fact, that energy supply on the parent ion can induce rapid D/H scrambling processes [25–27] before the fragmentation can take place. This is more prominent when the fragmentation efficiency is high as in the case of Q-TOF systems, which implement resonant dipolar radial excitation at high voltage amplitude [28]. Jorgensen et al. [29] have shown in a Q-TOF-MS that complete intramolecular randomization of all hydrogen atoms attached to nitrogen and oxygen in the amide functional groups with deuterium occurs in the gaseous peptide ion prior to its dissociation under low collisional energy activation conditions.

To date, no experimental or theoretical investigations exist, which explain the gas phase ion chemistry of oxocarboxylic acids and their fragmentation behaviour under low collision energy conditions. This paper provides a full gas phase chemical investigation of two model oxocarboxylic acids (5-oxohexanoic and 6-oxoheptanoic acid) on both experimental and theoretical levels. Strong evidences for the mediation role of ion-neutral complexes in characterizing specific anion fragmentation channels were obtained from DFT study described in detail in this paper. Experimental and theoretical evidences for intramolecular proton transfer event inside the anionic structure, which characterize a specific fragmentation channel of 6-oxoheptanoic acid anion, are shown.

2. Methods

2.1. Experimental

An orthogonal-acceleration time-of-flight mass spectrometer coupled to three linear quadrupoles for mass selection and fragmentation was used. The instrumental setup and the physical principles of operation are discussed in detail in a comprehensive review [30]. Fig. 1 gives a schematic representation of the instrument used.

The first quadrupole (Q1) acts as ion buncher. Quadrupole Q2 is for ion isolation based on mass-to-charge ratio. Q3 acts as a collision chamber, where the isolated ions of a specific m/z value can be kinetically accelerated for collision-induced dissociation experiments. The implementation of a reflectron is advantageous in extending the ion beam path (thus increasing the resolution) in addition to its important role in kinetic energy focusing.

Turbo-ionspray interface was used in the negative mode for ionization of the analyzed oxocarboxylic acids. The ionization source contains a heater probe orthogonally directed relative to the electrospray needle direction. Temperatures up to 500 °C can be used with this construction. At 400 °C, analytes can be injected at relatively high liquid flow rates up to 200 μL/min without significant signal intensity reduction.

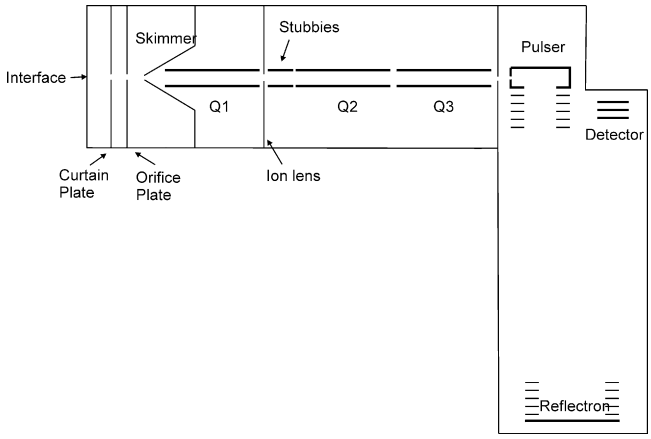

Fig. 1. Schematic view of the triple-quad-MS/MS-TOF hybrid system used in this study.

5-Oxohexanoic acid and 6-oxoheptanoic acid (97%) were purchased from Sigma–Aldrich Company and used without further purifications. Each analyte was separately dissolved in pure methanol (HPLC Lichrosolv Hypergrade, Merck). The methanolic solutions were injected at a concentration of 10 μM with a liquid flow rate of 100 μL/min under high temperature (400 °C) through the orthogonally directed heater gas for rapid solvent evaporization. Electrospray needle voltage was kept at −3.5 kV relative to the grounded curtain plate (which acts as a counter electrode). Ten scans were summed up in the multichannel acquisition mode (MCA). Unless otherwise indicated, no cone-voltage fragmentation (nozzle skimmer dissociation) was implemented prior to analysis. Collision-induced dissociation (CID) was performed on an isolated ion in Quadrupole Q3, which acts as a collision chamber filled with nitrogen as collision gas and has a relatively high pressure of 3×10^{-3} mbar. Several CID experiments were performed up to collision energy of 20 eV in the laboratory frame to obtain information about the threshold fragmentation values, at which specific fragment ions start to appear in the MS/MS spectrum. Ion transmission window for the accelerated ions through the quadrupoles is as follows (m/z = 45, 5%; m/z = 120, 45%; m/z = 180, 50%). This transmission window is best suited for the scanned mass range m/z = (40–350) Da.

2.2. Calculations

The electronic structure calculations were performed on a stand-alone computer using density functional theory, incorporated in Gaussian 03W program [31]. The hybrid DFT method B3LYP was implemented in combination with different basis sets. All geometry optimizations were performed using 6-31+G(d). Frequency calculations were also done for each optimized geometry using the same basis set 6-31+G(d) to obtain the zero point vibrational energy (ZPVE). This value is multiplied by the scaling factor 0.9804 to correct for vibrational anharmonicities. Single point energy (SPE) calculations were done using two theoretical levels of basis sets: 6-311+G(2d,p) and 6-

311++G(3df,3pd). The use of diffuse functions was important to represent the correct geometry of anionic species. Stability tests on all calculated structures were performed to ensure that the used wave function does represent the lowest energy solution of the SCF equations.

For geometry optimization, the Berny [32] analytical gradient optimization routines were used in combination with the GDIIS algorithm [33–35]. The requested convergence in the density matrix was 10^{-8} atomic units, the threshold value for maximum displacement was 0.0018 Å, and that for the maximum force was 0.00045 Hartree/Bohr. The nature of the stationary points was established by calculating and diagonalizing the Hessian matrix (force constant matrix). Transition structures were characterized through normal-mode analysis (frequency analysis). The transition vector associated with the unique imaginary frequency has been determined in each found transition state. This vector represents the eigenvector associated with the unique negative eigenvalue of the force constant matrix, which indicates that the found structure corresponds to a first order saddle point (transition state). In order to further check that the found transition state really connects two energy minima structures with each other (reactant with product), intrinsic reaction coordinate [36] (IRC) calculations in all found transition state geometries, were performed. For those cases, where energy barriers for intramolecular ionic transformations are too small (such as in pseudo-cyclization processes), IRCMax calculations [37] (reaction path transition state maximum energy location) were performed. Both IRC and IRCMax calculations were performed in mass-weighted internal coordinates [38]. All geometries of electronic structures calculated were rendered by GaussView program [39]. Mechanistic studies for isodesmic transformations (gas phase intramolecular rearrangements and ion fragmentation processes) are represented in this paper.

3. Results and discussions

3.1. Negative ion mass spectra of 6-oxoheptanoic acid

Only one primary ion at $m/z = 143$ was observed in the TOF mass spectrum of 6-oxoheptanoic acid, when electrospray ionization in the negative ion mode was applied. This ion corresponds to the deprotonated form $[M - H]^-$ of the oxocarboxylic acid. Fig. 2 shows CID mass spectra of this parent ion $m/z = 143$ at three different collision energies (10, 15 and 20 eV applied, in the laboratory frame).

From the measured mass differences between the parent ion and the fragment ions, water elimination $[M - H–H_2O]^-$ $m/z = 125$ and CO_2 loss $[M - H–CO_2]^-$ $m/z = 99$ are two different channels delineating the fragmentation behaviour of the parent ion $[M - H]^-$ $m/z = 143$.

The measured mass difference between the primary fragment ion $[M - H–H_2O]^-$ $m/z = 125$ and the secondary fragment ion $m/z = 83$ represents the sum formula C_2H_2O. Thus, carbene CH_2=C=O elimination could be deduced from the primary fragment ion $[M - H–H_2O]^-$ $m/z = 125$.

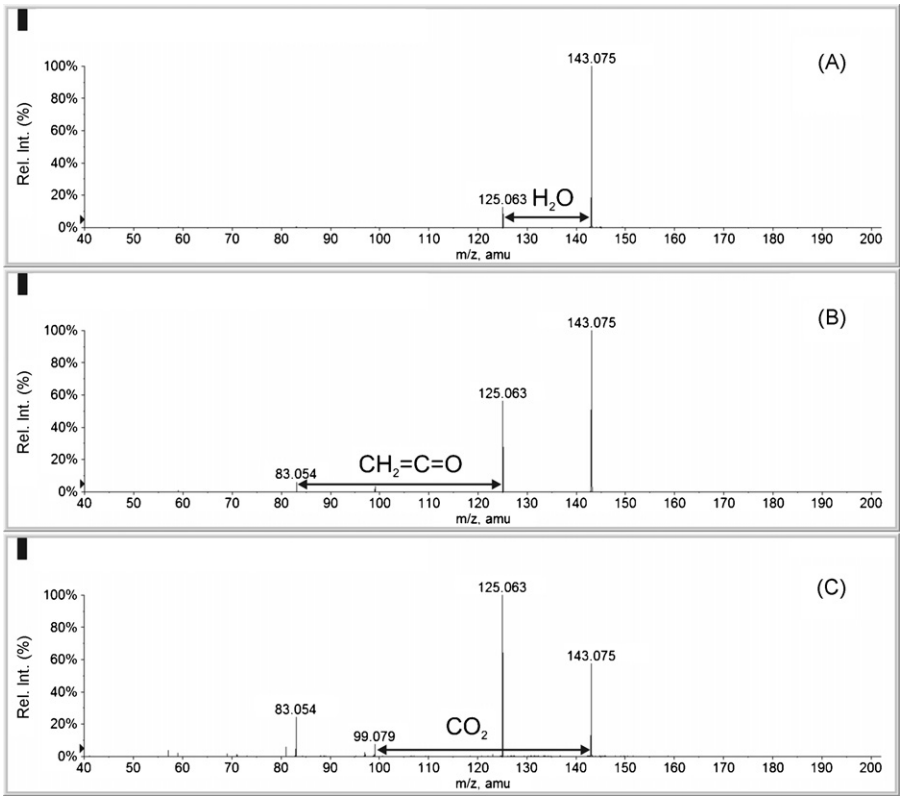

Fig. 2. CID mass spectra of parent ion $[M - H]^-$ $m/z = 143$ of 6-oxoheptanoic acid performed at (A) 10 eV; (B) 15 eV; (C) 20 eV. Signals above 5% are shown with their measured masses.

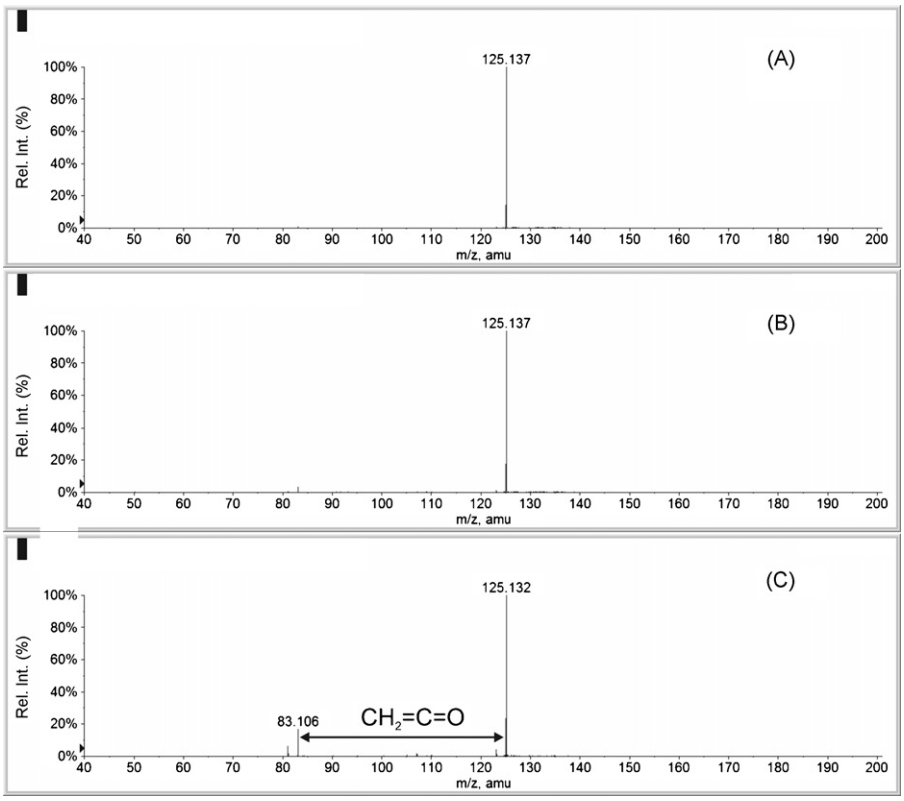

Fig. 3. Selected primary fragment ion $[M-H–H_2O]^-$ $m/z=125$ dissociation at three different collision energies: (A) 10 eV; (B) 15 eV; (C) 20 eV. The secondary fragment ion $m/z=83$ is generated to 20% when 20 eV activation energy was applied.

Evidence, that the ion $m/z=83$ is formed from $m/z=125$, is provided in Fig. 3, which illustrates the result of the following experiment: the parent ion $m/z=143$ is fragmented in the region between the orifice plate and skimmer by applying high acceleration electric field (cone-voltage induced dissociation) and the primary fragment ion $[M-H–H_2O]^-$ $m/z=125$, which is generated and then accelerated throughout the skimmer region was selected in the second quadrupole and collisionally fragmentated in the third quadrupole (which acts as a collision chamber) producing ion $m/z=83$.

The exact mass difference measured between $m/z=125$ and $m/z=81$ does not correspond to the loss of CO_2 from ion $m/z=125$ but to the loss of C_2H_4O. Thus, ion $m/z=83$ can eliminate H_2 to form $m/z=81$, since no direct C_2H_4O elimination (in the form of acetaldehyde or epoxide ring) could be logically determined through the consideration of the mechanistic frag-

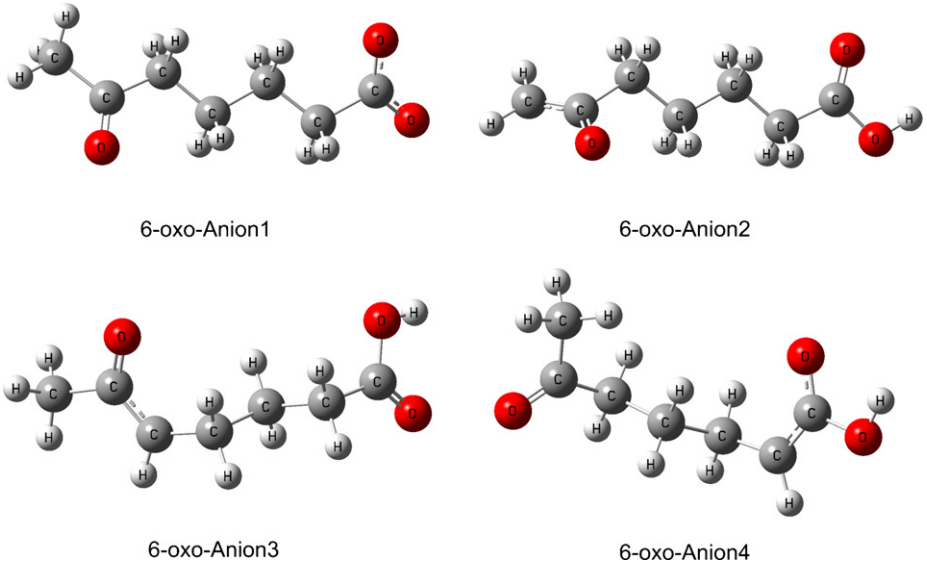

Fig. 4. Optimized structures (B3LYP/6-31+G(d)) of four different isomers of anion $[M-H]^-$ $m/z=143$ of 6-oxoheptanoic acid.

Table 1
Deprotonation potential (298 K) of isomeric anions of 6-oxoheptanoic acid

#	Name	*E* (Hartree)	DP B3LYP/6-311+G(2d,p) (kcal/mol)
0	6-Oxoheptanoic acid neutral	−499.64227769	0.0
1	6-oxo-Anion1	−499.09729436	342.0
2	6-oxo-Anion2	−499.06438941	362.6
3	6-oxo-Anion3	−499.07022826	359.0
4	6-oxo-Anion4	−499.06800136	360.4

mentation pathways studied by DFT. However, it is important to note, that no CO_2 loss can take place starting from the primary fragment ion $[M - H–H_2O]^-$ $m/z = 125$ as discussed above.

Combined Skimmer-Quadrupole Q3 CID fragmentation experiment, whose results are shown in Fig. 3, also illustrates, that ion $m/z = 99$ generated by the fragmentation of $m/z = 143$ (as shown in Fig. 2) is not a secondary fragment ion produced from the primary fragment ion $[M - H–H_2O]^-$ $m/z = 125$. Thus, CO_2 loss takes place directly from the parent ion $[M - H]^-$ $m/z = 143$.

3.2. DFT mechanistic studies for the anionic fragmentation pathways related to 6-oxoheptanoic acid

3.2.1. Isomeric anions and water elimination

From a theoretical point of view, there are four different positions, where deprotonation can take place in the neutral molecule of 6-oxoheptanoic acid. Fig. 4 shows the optimized geometries of these four different isomers. While Anion1 represents the deprotonation from the carboxyl group, Anion4 shows the optimized geometry, when the neutral is deprotonated from α C position relative to the carboxyl group. Anion2 represents acetyl deprotonation, while Anion3 shows the geometry of the anion formed, when the neutral is deprotonated from the α C internal position relative to the acetyl group. All these four different anionic isomers play a major role in our discussion on fragmentation mechanisms illustrated below. A deprotonation relative to either carbonyl or carboxyl groups can be stabilized through electron delocalization (resonance) in the generated enolate moiety.

Table 1 lists the deprotonation potential of the four isomeric anions of 6-oxoheptanoic acid shown in Fig. 4.

It can be concluded from Table 1 that deprotonation of the carboxyl group represents the most probable (thermodynamically favourable) event, that is expected to take place in the electrospray ionization source for ionization of 6-oxoheptanoic acid in the negative operation mode. All other anionic isomers have relatively higher deprotonation potentials but their values are close to each other (about 360 kcal/mol).

If we assume, that isomeric anions other than 6-oxo-Anion1 cannot be directly generated through electrospray ionization process, we cannot exclude the fact, that 6-oxo-Anion1 can undergo rapid ion-molecule reactions with 6-oxoheptanoic acid neutrals to generate other anionic isomers (listed in Table 1). Those gas phase ion-molecule reactions can take place on a microsecond time scale, since the collision frequency between particles is high at atmospheric pressure occurring in the ionization source.

Mechanistic study of water elimination from $[M - H]^-$ $m/z = 143$ will be presented first, since it represents a major fragmentation channel as shown experimentally in Fig. 2. CID fragmentation patterns (Fig. 2) obtained by applying three different collision energies clearly show, that water elimination is energetically more favourable than CO_2 ejection.

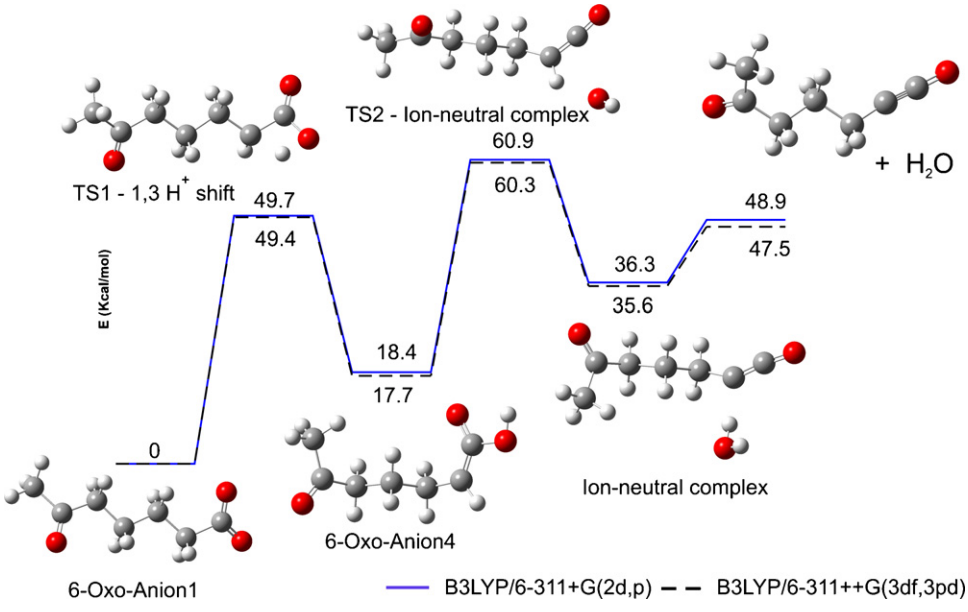

Fig. 5. Potential energy curves for water elimination from $[M - H]^-$ $m/z = 143$; SPE calculated by B3LYP/6-311+G(2d,p) and B3LYP/6-311++G(3df,3pd).

Fig. 5 shows a potential energy curve for water elimination from 6-oxo-Anion1 isomer.

As shown in Fig. 5, water elimination is a two step process. In the first step, 6-oxo-Anion4 isomer should be generated by a 1,3 proton shift. Once formed, 6-oxo-Anion4 isomer can undergo a gas phase rearrangement to generate a ketene and an OH^- ion, which remains bonded through a non-covalent interaction. OH^- can then abstract a proton from the neutral ketene to generate a ketene anion and water. The formed ketene anion can be stabilized through electron delocalization.

1,3-Proton shift has a forward energy barrier of 49.7 kcal/mol on the B3LYP/6-311+G(2d,p) level of theory. Due to the fact that multi-acceleration events can occur throughout the triple quadrupole region, where the acceleration electric field for fragmentation can arise, formed 6-oxo-Anion4 isomer (as a result of a 1,3-proton shift) can be further accelerated to generate an ion-neutral complex, from which water can be eliminated. The forward energy barrier for the second transition state found is $60.9 - 18.4 = 42.5$ kcal/mol on the B3LYP/6-311+G(2d,p) level of theory. The reverse energy barrier is +24.6 kcal/mol and this energy release can be partitioned through different energy forms. Thus, the translational energy release can be deduced through the existence of this reverse energy barrier in the case of both TS1 and TS2, which helps OH^- to move within the ion-neutral complex for a proton abstraction. Translational energy is available to separate water neutral from the formed ketene anion.

In all potential energy curves shown, single point energy calculations SPE were performed using two different basis sets: 6-311+G(2d,p) (solid line) and 6-311++G(3df,3pd) (dashed line). Thus two potential energy curves are obtained for each fragmentation channel. Both curves show the same trend along the reaction coordinate.

3.2.2. CO_2 elimination

The loss of CO_2 along the potential energy curve is presented in Fig. 6. Since there is no positive reverse energy barrier for CO_2 removal from 6-oxo-Anion1 isomer, there is no dynamic release of translational energy that could force the CO_2 neutral and the anion to separate. This explains the large discrimination between the two fragmentation pathways (water elimination versus CO_2 removal), although the energy demand for CO_2 removal is lower than that required for water elimination (compare forward energy barriers in Figs. 6 and 5).

Since C_2H_4 removal depends on CO_2 loss and CO_2 removal is inhibited, no C_2H_4 removal can be observed experimentally (Fig. 2). This is apparent from the lack of $m/z = 71$ ion generation in Fig. 2.

The anionic rest without CO_2 is instable, due to the fact that a negative charge after CO_2 loss would reside on the terminal CH_2 group of the chain and the electrons cannot undergo delocalization to stabilize the generated anionic system. Electron delocalization cannot be even enabled, if C_2H_4 is simultaneously removed with CO_2 in a concerted mechanism, since the formed anionic rest in this case is still far away from resonance stabilization compared to anionic enolate system. Enolate ion cannot be generated neither in successive nor in concerted mechanistic event.

3.2.3. Ketene CH_2=C=O elimination

As indicated in Section 3.1 and confirmed experimentally in Fig. 3, ketene CH_2=C=O is removed from the ion $[M - H–H_2O]^-$ $m/z = 125$, when the latter ion is further accelerated in the acceleration electric field, sustained between the first and the third quadrupole in the CID experiment.

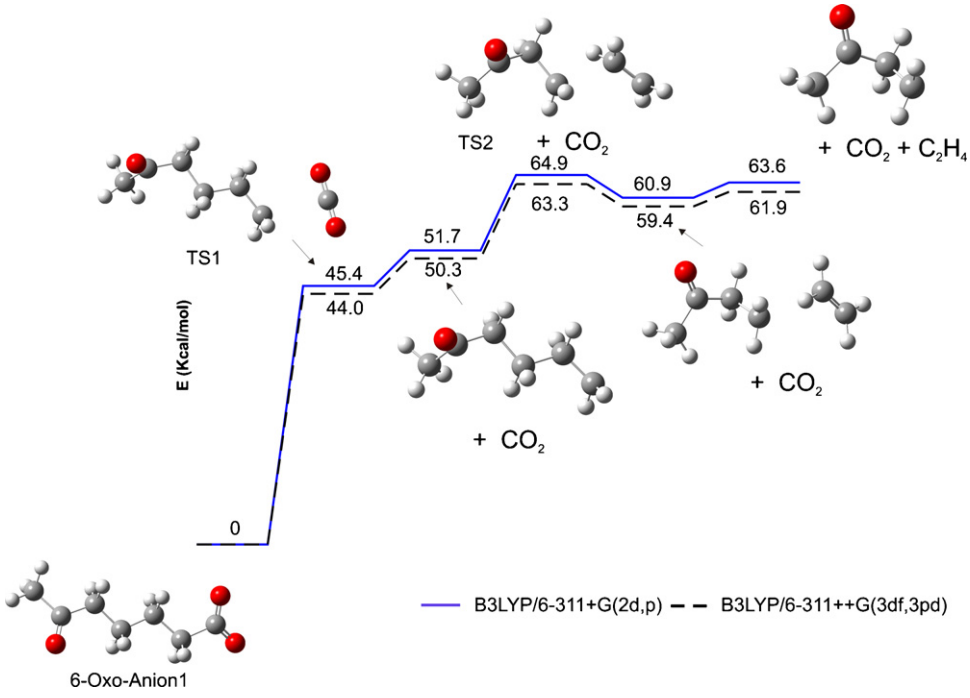

Fig. 6. Potential energy curves for CO_2 release and for theoretical C_2H_4 removal.

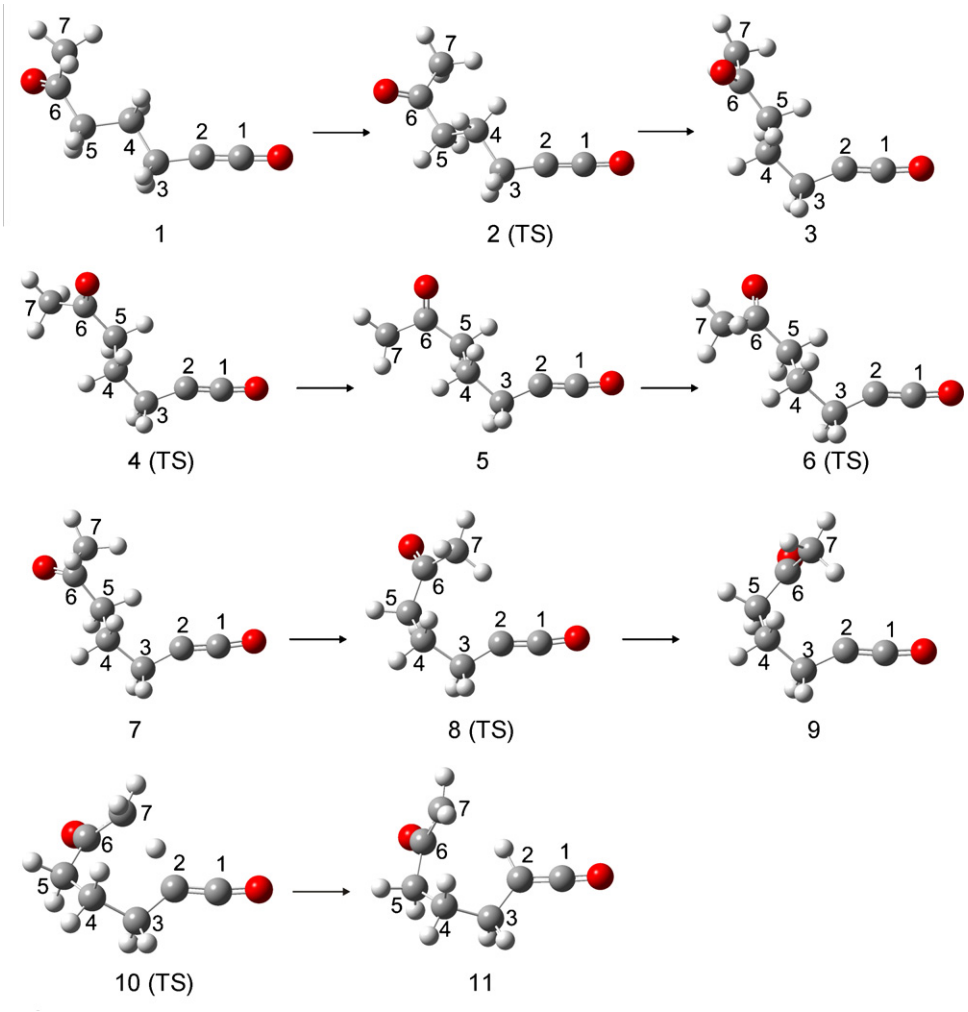

Fig. 7. Structural conformational analysis of the ketene anion $m/z = 125$ $[M - H–H_2O]^-$ towards pseudo-cyclization and rearrangement through proton transfer.

As shown previously in the far right hand structure of Fig. 5, the optimized structure of $[M - H–H_2O]^-$ formed directly after water elimination does not enable a small ketene neutral (CH_2=C=O) to be directly eliminated from the anion. Thus, a rearrangement must occur (Eq. (2)) and it includes a proton transfer from the terminal acetyl methyl group to the internal carbene carbon atom, which bears a substantial partial negative charge. This creates a carbene terminal in the end anionic structure after proton transfer. The carbene terminal generated from the acetyl group of anion $[M - H–H_2O]^-$ can then be eliminated to produce anion $[M - H–H_2O–C_2H_2O]^-$ $m/z = 83$.

A strong evidence exists, which confirms the formation of the ejected ketene CH_2=C=O from the acetyl moiety. Collisional fragmentation of the parent ion $[M - H]^-$ of heptanoic acid (or other acyclic monocarboxylic acids with different carbon chain lengths) does not eject CH_2=C=O. This indicates that the oxygen atom included in the eliminated neutral sum formula C_2H_2O does not originate from the carboxyl functional group of 6-oxoheptanoic acid parent ion $[M - H]^-$ but originates from the acetyl terminal.

For the proton transfer to take place (as shown in Eq. (2)), a special conformer of anion $[M - H–H_2O]^-$ $m/z = 125$ (structure 9 in Fig. 7) must be formed starting from that anion generated directly after water elimination (structure 1 in Fig. 7).

Fig. 7 shows the different conformational geometries of anion $[M - H–H_2O]^-$ $m/z = 125$, optimized on the B3LYP+G(d) level of theory, which lead finally to the intramolecular proton transfer discussed above.

Fig. 8 shows the energy profile for the conformational changes that take place on anion $[M - H–H_2O]^-$ $m/z = 125$ before proton transfer and ketene elimination occur to produce $[M - H–H_2O–C_2H_2O]^-$ ion $m/z = 83$.

The energy profile in Fig. 8 shows the limit of the DFT-B3LYP in determining energies of minima and transition state geometries, even when the highest B3LYP++G(3df,3pd) SPE is employed. It is known that the accuracy of DFT calculations is within 1–2 kcal/mol for single point energy determinations. The first step of the pseudo-cyclization process has 2.4 kcal/mol forward energy barrier. Although optimized structures 4 and 8 in Fig. 7 were found as transition states (with a characteristic transition vector for each TS connecting the required minima for the dihedral angle reorientations), they have a small but negative reverse energy barrier. However, these energy values are too small and lie within the errors of DFT single point energy calcu-

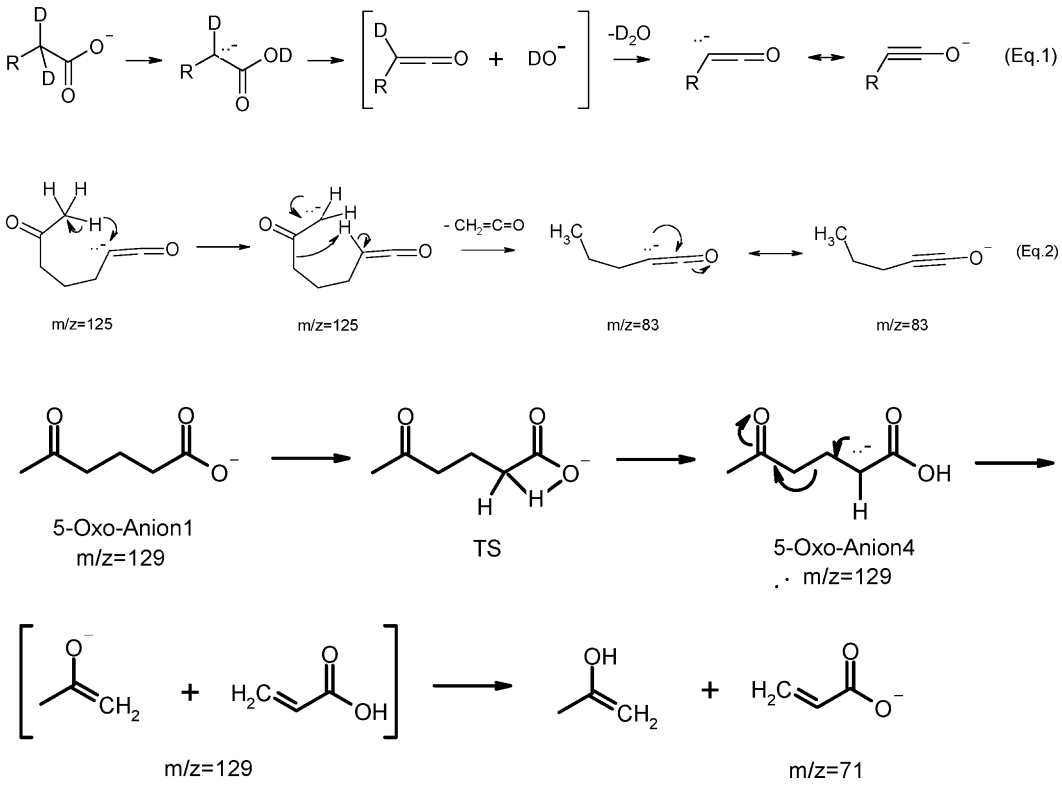

Scheme 1. Proposed mechanism for the generation of the minor fragment ion $m/z = 71$.

lations. It is important to note, however, that the energy profile shown in Fig. 7 gives evidence that the proposed conformational change of the ketene $[M - H–H_2O]^-$ $m/z = 125$ (structure 1 in Fig. 7) can easily take place before proton transfer occurs, since the energetic demand for this overall conformational change is too small and feasible within the CID experiment.

A characteristic transition vector (with one imaginary frequency) along the reaction coordinate was found for each transition state shown in Fig. 7. IRC calculations (performed starting from each optimized transition state) prove that each found transition state really connects the correct corresponding energy minima structures with each other through the whole conformational change and the final proton transfer illustrated in Fig. 7.

Table 2 shows the dihedral angles involved in the conformational change for pseudo-cyclization.

The conformational change begins with rotation of the acetonyl moiety around C3–C4 to yield conformer 3. Acetyl group can then rotate around the C5–C6 bond to generate conformer 5. Additional rotation around the C5–C6 bond generates structure 7. Rotation around the C4–C5 bond yields conformer 9, which renders the methyl substituent of the acetyl group in the proximity of C2. The distance between C2 and the nearest proton in conformer 9 is just 253 pm. The negative charge on C2 favours the proton transfer with a low energy barrier of

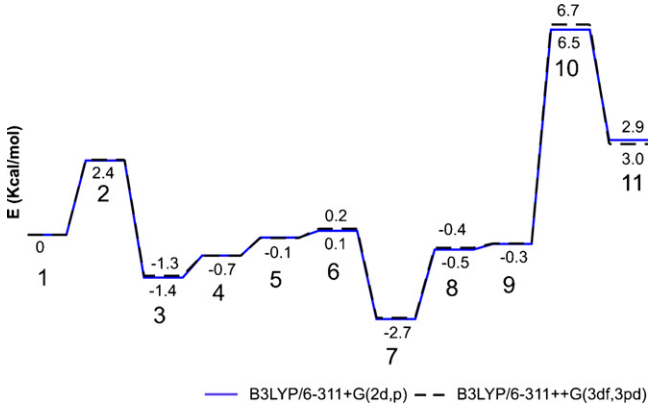

Fig. 8. Energy profile for pseudo-cyclization rearrangement of the ketene anion (formed after water elimination) and the proton transfer from one terminal to the other one (see text).

Table 2
Dihedral angles, which are important in the conformational change shown in Fig. 7

Structure #	D1 = C2C3C4C5	D2 = C3C4C5C6	D3 = C4C5C6C7
1	−177.6	178.8	−60.2
2	121.8	−177.2	79.2
3	55.6	−173.7	−168.0
4	56.2	178.3	−113.8
5	56.6	172.5	−94.4
6	61.7	−178.2	−23.4
7	59.3	−168.2	58.3
8	63.8	−92.1	3.4
9	64.8	−73.6	−34.4
10	74.8	−60.5	−24.8
11	75.9	−71.1	−30.5

Dihedral angle $D = -180$ is equivalent to $D = 180$.

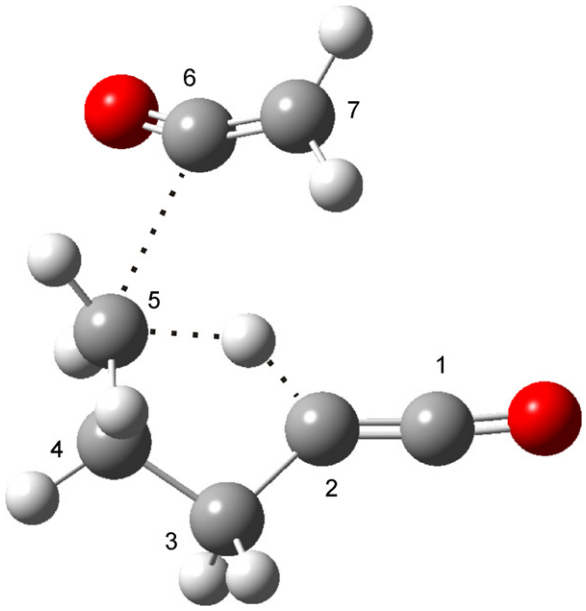

Fig. 9. Optimized transition state structure for CH_2=C=O elimination from the big ketene anion $m/z = 125$ (structure 11 in Fig. 6).

just 6.5 kcal/mol (6-311+G(2d,p)). The conformational change discussed and shown in Fig. 7 is necessary prior to proton transfer. No CH_2=C=O ketene elimination can take place if proton transfer does not occur (Eq. (2)).

Structure 10 in Fig. 7 represents an optimized geometry of the transition state, which illustrates the transfer of a proton from C7 to C2. Once structure 11 is formed, a terminal CH_2=C=O moiety is generated. This small ketene (CH_2=C=O) can then be eliminated in a concerted mechanism shown in Fig. 9.

As C6 departs away from C5, the proton attached to C2 shifts toward C5 (proton transfer event concomitant with ketene elimination). The driving force for this concerted mechanism can be explained as follows: when C6 departs away from C5, a negative charge is formed on C5 and this negative charge is not stable in this terminal position. Since there is a pseudo-5-membered ring C2–C3–C4–C5–H, the proton attached to C2 can be attracted by the negative charge on C5. The proton transfer from C2 to C5 shifts the negative charge from C5 to C2 synchronously with CH_2=C=O neutral elimination. Negative charge formation on C2 creates a more stable overall anionic system, since the negative charge on C2 can be stabilized through resonance (electron delocalization) as shown previously in Eq. (2).

The dihedral angle C1–C2–H–C5 is 178.2° and the dihedral angle C2–H–C5–C6 is 177.6°. The proton shown between C2 and C5 in Fig. 9 is the shifted proton. From those two dihedral angles, it is clear that both proton transfer and C6 departure (ketene elimination) take place in the same paper plane. The C7–C6–O angle is 157° and this indicates a great departure from C7–C6–O angle of 126.5° for sp^2 hybridized carbonyl carbon atom in structure 11 in Fig. 7.

Fig. 10 shows the energy profile for the proton transfer and CH_2=C=O elimination. The energy barrier for the intramolecular proton transfer (7 kcal/mol) is noticeably lower than that for ketene CH_2=C=O elimination. Once eliminated, CH_2=C=O can be attracted to the internal carbene carbon atom, which bears a negative charge, to form an ion-neutral complex (see Fig. 10). This complex can dissociate easily by applying 8.4 kcal/mol to generate K3 anion $m/z = 83$. The net fragmentation reaction shown in Fig. 10 is endothermic, as expected.

Ketene anion K3 $[M - H–H_2O–C_2H_2O]^-$ $m/z = 83$ can eliminate H_2, when the collision energy reaches 20 eV in the laboratory frame (Fig. 3).

There are three pathways, through which H_2 can be eliminated from ketene K3 (Fig. 11).

Pathway EV2 illustrates vicinal H_2 elimination from the internal C–C bond. Pathway EV1 illustrates vicinal H_2 elimination from external C–C bond of the ketene anion (as shown in Fig. 11). In pathway E1, geminal H_2 elimination from the external methyl group of the ketene is shown. No transition states for geminal H_2 eliminations from internal methylene moieties could be found.

Vicinal H_2 elimination from the internal C–C bond does not only have the lowest energy barrier but also yields the lowest energy minimum. So pathway EV2 is thermodynamically the most favourable fragmentation channel of the ketene $[M - H–H_2O–C_2H_2O]^-$ $m/z = 83$ to yield anion $m/z = 81$ after H_2 elimination.

Geminal H_2 removal from external methyl group (pathway E1) has a forward energy higher, which lies between that of EV1 and EV2. However, the reverse energy barrier for pathway E1 is nearly negligible, since the product fragment ion generated through pathway E1 is very high in energy (instable).

3.3. Negative ion mass spectra of 5-oxohexanoic acid

Only one primary ion $m/z = 129$ was observed in the TOF mass spectrum of 5-oxohexanoic acid, when electrospray ionization in the negative ion mode was applied. This ion corresponds to the deprotonated form $[M - H]^-$ of the oxocarboxylic acid. Fig. 12 shows CID mass spectra of the parent ion $m/z = 129$ at three different collision energies (10, 15 and 20 eV).

From the measured mass differences between the parent ion and the fragment ions, water elimination $[M - H–H_2O]^-$ $m/z = 111$ and C_4H_6O neutral elimination from $[M - H]^-$ producing anion with $m/z = 59$ could be discerned. CO_2 elimination product ion $m/z = 85$ could not be detected. Thus, CO_2 loss is suppressed relative to C_4H_6O elimination (as seen in Fig. 12A). The latter fragmentation type is highly favourable and the product ion $[M - H–C_4H_6O]^-$ $m/z = 59$ appears noticeably even at a collision energy of 10 eV.

When the activation energy is raised to 15 eV in the laboratory frame, $[M - H–CO_2]^-$ fragment ion $m/z = 85$ is still not observable. We will provide evidence later (through DFT elucidated reaction mechanisms), that the absence of a signal corresponding to the mentioned ion at higher collision energies is not due to a high forward energy barrier, which prevents the formation of the product ion $[M - H–CO_2]^-$, but due to dissociation of the parent ion $[M - H]^-$ in a concerted mechanism to yield $[M - H–CO_2–C_2H_4]^-$ $m/z = 57$ directly.

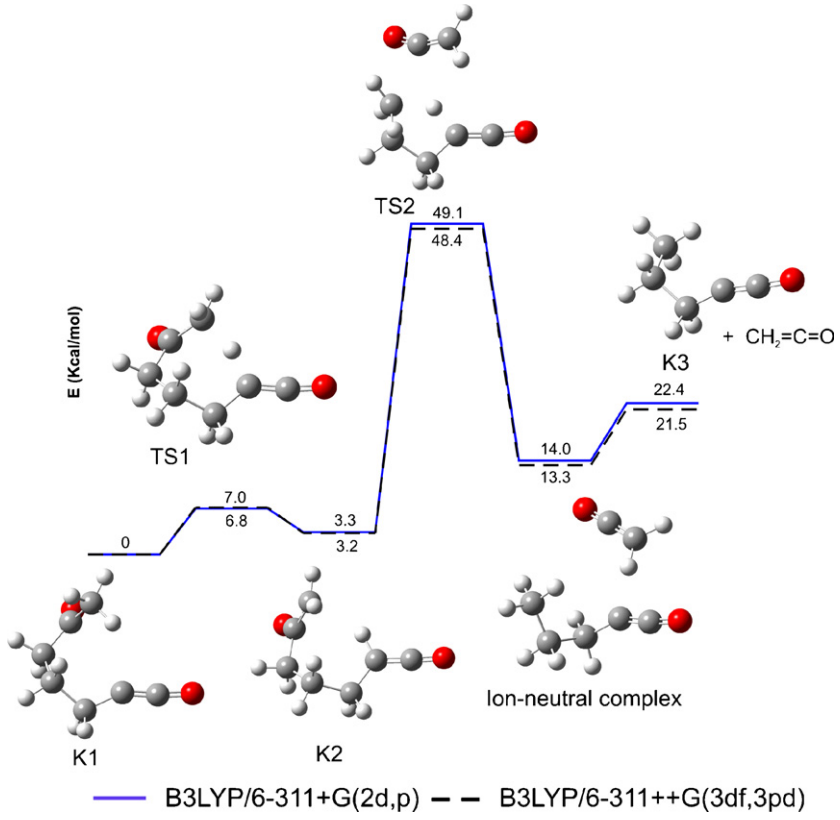

Fig. 10. Energy profile for proton transfer and ketene CH_2=C=O elimination.

In our DFT discussion provided later for elucidation of anionic reaction mechanisms of 5-oxohexanoic acid, we will give a thermodynamic evidence, which indicates that the fragment ion $m/z = 57$ (seen in Fig. 12B) is not produced from anion $m/z = 59$ through H_2 elimination, but directly from the parent anion $[M - H]^-$ $m/z = 129$ through synchronous CO_2 and C_2H_4 eliminations.

Indeed, the measured mass difference between fragment ion $m/z = 57$ and the parent ion $m/z = 129$ (72.018 Da) refers to a neutral molecule having sum formula $C_3H_4O_2$ with an absolute

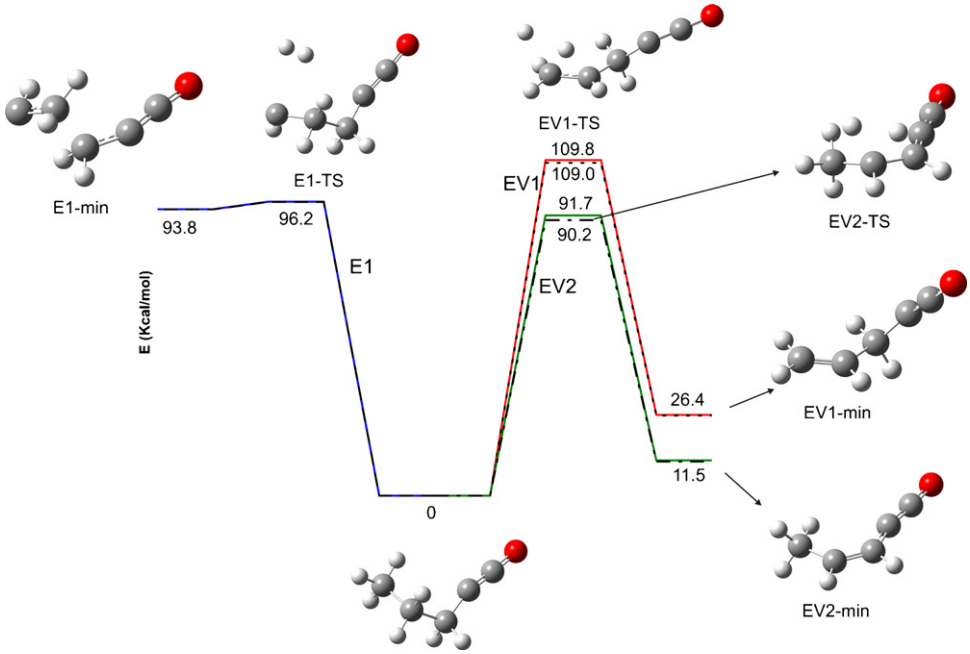

Fig. 11. Energy profiles for three different theoretical pathways for H_2 elimination from ketene anion $[M - H–H_2O–C_2H_2O]^-$ $m/z = 83$ (shown with 0 kcal/mol) on the diagram. Continuous lines represent B3LYP/6-311+G(2d,p); dashed lines represent B3LYP/6-311++G(3df,3pd) level of theory for single point energy calculations.

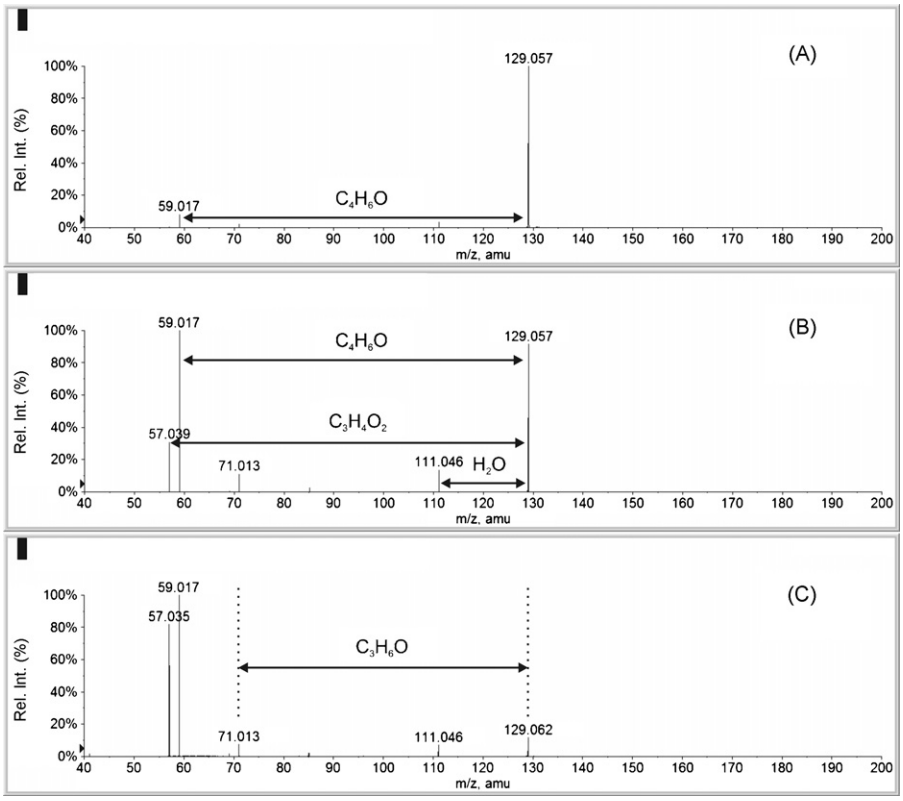

Fig. 12. CID mass spectra of parent ion $[M-H]^-$ $m/z = 129$ of 5-oxohexanoic acid performed at (A) 10 eV; (B) 15 eV; (C) 20 eV. Signals above 5% are shown labeled.

mass deviation of just 3 mDa at a TOF resolution of 3200. Other candidates (such as C_6, C_2O_3 shown in Table 3) for the same measured neutral mass difference (72.018 Da) are of no logical and chemical fragmentation meanings. The neutral C_4H_8O has a mass deviation by more than a factor of 10 higher than the first candidate.

3.4. DFT mechanistic studies for the anionic fragmentation pathways related to 5-oxohexanoic acid

3.4.1. Isomeric anions and water elimination

Similar to what is indicated previously in Section 3.2.1 in the case of 6-oxoheptanoic acid, there are several possible deproto-

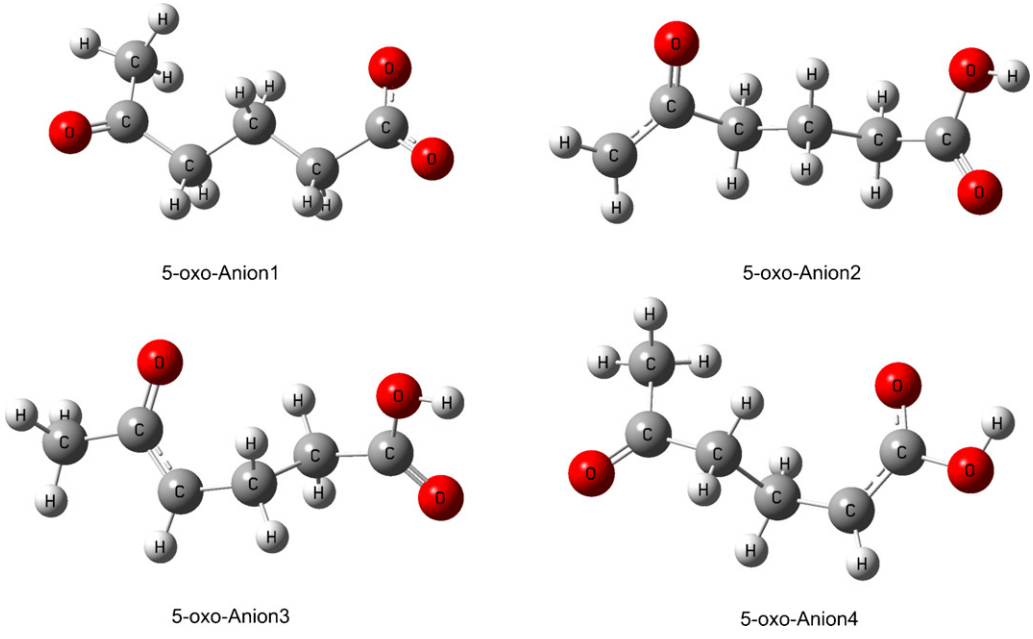

Fig. 13. Optimized structures (B3LYP/6-31+G(d)) of four different isomers of anion $[M-H]^-$ $m/z = 129$ from 5-oxohexanoic acid.

Table 3
Different candidates with nominal $m/z = 72$

Neutral candidate	Neutral sum formula	Calculated m/z (Da)	Mass deviation (mDa)
1	$C_3H_4O_2$	72.0211	−3.1
2	C_6	72	18.0
3	C_2O_3	71.9847	33.3
4	C_4H_8O	72.0575	−39.5

Table 4
Deprotonation potentials (298 K) of isomeric anions $[M - H]^-$ of 5-oxohexanoic acid

#	Name	E (Hartree)	DP B3LYP/6-311+G(2d,p) (kcal/mol)
0	5-Oxohexanoic acid neutral	−460.345056	0.0
1	5-oxo-Anion1	−459.804951	338.9
2	5-oxo-Anion2	−459.769807	361.0
3	5-oxo-Anion3	−459.777002	356.5
4	5-oxo-Anion4	−459.774393	358.1

nation sites in 5-oxohexanoic acid. Fig. 13 shows the optimized geometries of anions of 5-oxohexanoic acid deprotonated from different sites.

As indicated in Table 4, deprotonation at the carboxyl group is the most thermodynamically favourable ionization event. The deprotonation potential of all other anionic isomers is noticeably higher. However, 5-oxo-Anion4 isomer can be produced from 5-oxo-Anion1 through a 1,3 intramolecular proton shift in an endothermic transformation (see below). Other anionic isomers can be generated through ion-molecule gas phase reactions in the ionization source working at atmospheric pressure.

Fig. 14 shows the energy profile which illustrates the mechanism of water elimination from $[M - H]^-$ anion $m/z = 129$ of 5-oxocarboxylic acid.

As seen in Fig. 14, water elimination from 5-oxo-Anion1 is a two step process, which includes a 1,3 proton shift in the first step (through a forward energy barrier of 49.2 kcal/mol) to produce the isomer 5-oxo-Anion4. Once generated, isomer 5-oxo-Anion4 can be converted to a neutral ketene releasing an OH^- ion, which has enough kinetic energy to rotate around an axis (passing through the internal carbene C-atom and oriented perpendicular to the paper plane) to abstract a proton from the ketene and produce an ion-neutral complex between kenete anion and water neutral. The transition vector accompanied by the identified transition state TS2 proves the rotation of OH^- to approach the ketene hydrogen atom.

A new ion-neutral complex between water and the resultant ketene anion (formed after proton abstraction by OH^-) is formed and the optimized geometry is also shown in Fig. 14. No imaginary frequency is associated with this water–ketene anion complex so that it represents an energy minimum along the potential energy curve. 12 kcal/mol (on the B3LYP/6-311+G(2d,p) level of theory) is required to dissociate this complex to eliminate water and generate the ketene anion $[M - H–H_2O]^-$ $m/z = 111$.

From Fig. 14 it can be concluded that the forward energy barrier required to be overcome, for Anion1 to Anion4 transition (1,3 H^+ shift indicated by TS1) is lower than the energy barrier needed to generate {ketene anion–water} ion-neutral-complex, through which water elimination occurs. Due to the fact, that water loss was experimentally observed, even starting from 10 eV collision energy, provides evidence that 60.3 kcal/mol = 2.61 eV needed to overcome TS2 in Fig. 14 is

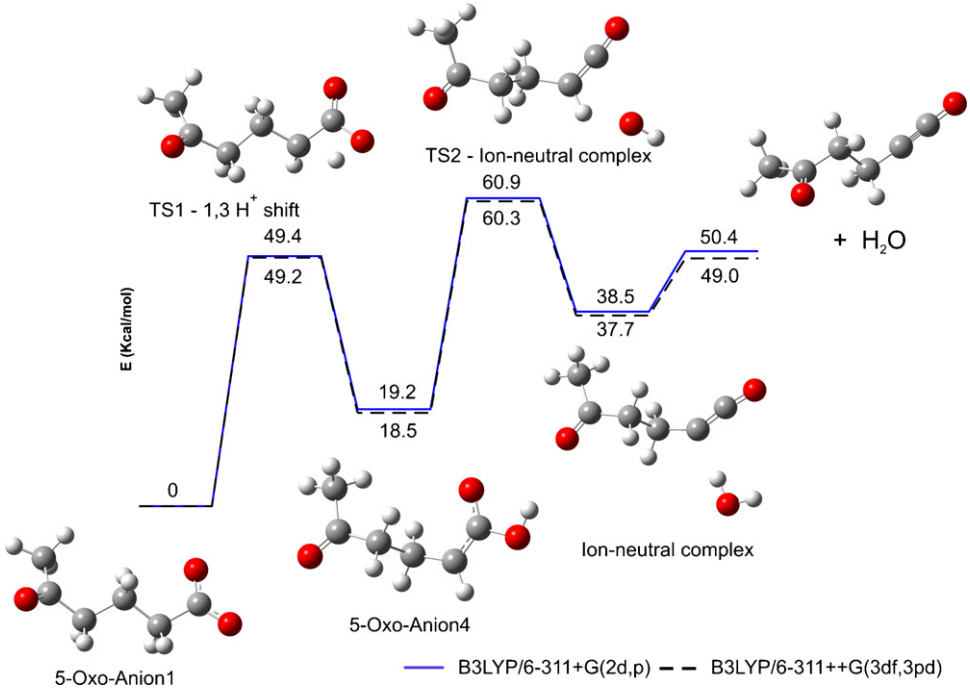

Fig. 14. Energy profile of water elimination from 5-oxo-Anion1 generated directly in the ionization source.

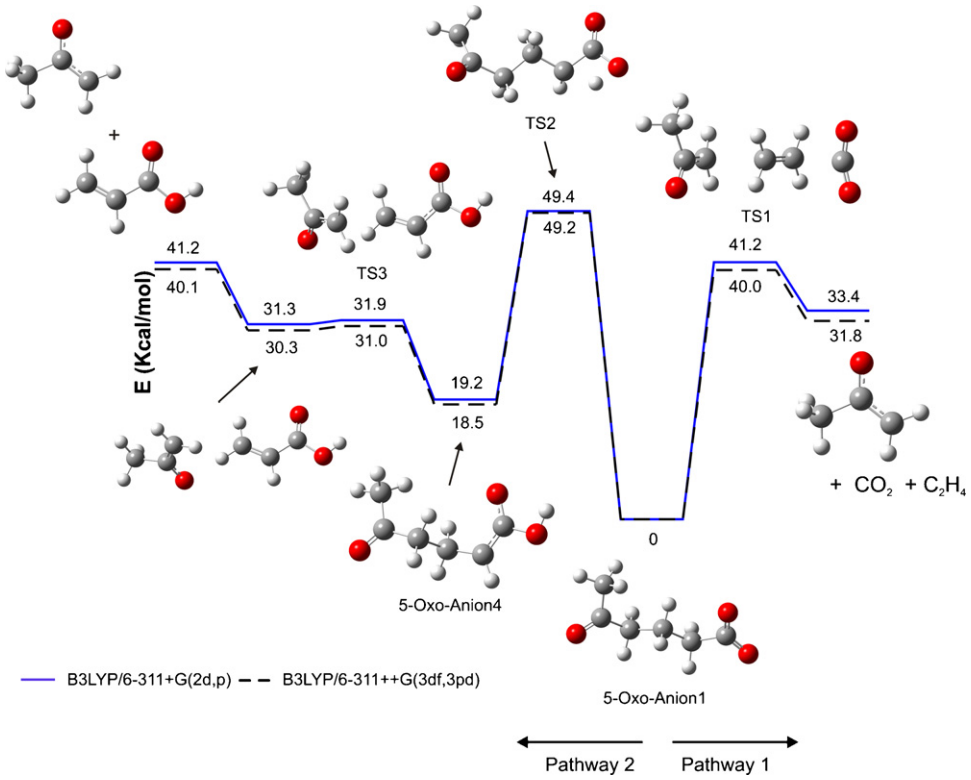

Fig. 15. Potential energy diagram for concerted CO_2 and $CH_2{=}CH_2$ elimination from 5-oxo-Anion1 (pathway 1) and for acetonyl anion generation $m/z = 57$ from 5-oxo-Anion4 isomer (pathway 2).

sustained through a collision energy of 10 eV. Thus the magnitude of internal energy deposition from kinetic acceleration electric field in our triple quadrupole system can reach 26%. It is known, that the percentage of internal energy deposition in triple quadrupole acceleration systems are higher relative to that of ion traps [40], although the pressure conditions in the collisional activation chambers (for CID) are nearly the same. Linear ion acceleration gives higher kinetic to internal energy conver-

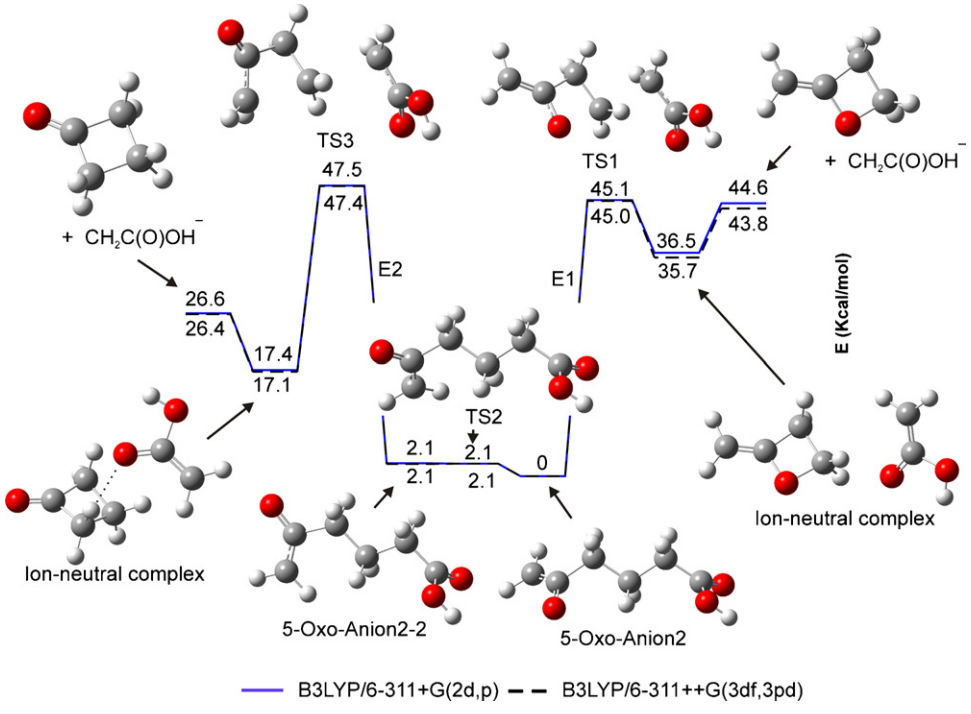

Fig. 16. Energy profile for cyclization of 5-oxo-Anion2 isomer to release anion $m/z = 59$.

sion factor than MS-analyzers, which apply radial components to ion movements.

If TS2 must be overcome to eliminate water and provided that water elimination was experimentally observed in CID experiments, the internal energy deposited by ion kinetic acceleration must enable the 1,3 proton shift prior to water elimination. Thus, there is a correlation between experimental measurements and theoretical energy requirements calculated on the B3LYP/6-311++G(3df,3pd) level of theory.

3.4.2. Synchronous CO_2 and ethylene elimination and second way to generate acetonyl anion

Fig. 15—pathway 1 shows the energy profile of synchronous CO_2 and C_2H_4 elimination from $[M-H]^-$ anion of 5-oxohexanoic acid.

The identified transition state TS1, which is responsible for ion $m/z = 57$ formation in the CID mass spectrum, is shown in Fig. 15. The transition vector of this transition state reveals a concerted mechanism, by which both CO_2 and $CH_2{=}CH_2$ are eliminated synchronously from the isomer 5-oxo-Anion1 $[M-H]^-$ $m/z = 129$.

This concerted mechanism deduced from TS1 geometry can be explained by noticing that the produced anion rest is an enolate ion, which is very stable due to electron delocalization. CO_2 removal alone would let a negative charge to reside on a terminal unbranched methylene group, which is not stable due to a lack of electron delocalization. Thus, the concerted mechanism in pathway 1 takes place in an attempt of the system to reach stable fragment anion (acetonyl enolate). This is in agreement with the experimental evidence (Fig. 12) for the lack of CO_2 elimination product ion $m/z = 85$ in the whole collision energy range (10–20 eV) within the CID experiments.

No deuterium labeling experiments can be helpful in this case to distinguish between pathway 1 and pathway 2 (shown in Fig. 15), since the acetonyl anion observed in the CID mass spectra originates from the same terminal part of the parent anion $[M-H]^-$ $m/z = 129$ regardless whether it is in the form of 5-oxo-Anion1 or 5-oxo-Anion4 isomer.

It is obvious from Fig. 15 that pathway 1 is thermodynamically more favourable relative to pathway 2, since the forward energy barrier height for pathway 1 (TS1 = 41.2 kcal/mol on the 6-311+G(2d,p) level) is lower than that necessary to initiate pathway 2 (TS2 = 49.4 kcal/mol). Moreover, the energy sum of all the products produced as a result of pathway 1 is lower than that for the products generated through pathway 2. Thus, we believe that acetonyl anion $m/z = 57$ observed in the CID mass spectra shown in Fig. 12B and C is formed through the concerted mechanism indicated as pathway 1 in Fig. 15.

3.4.3. Cyclization of 5-oxo-Anion2 isomer

As can be seen in Fig. 16, the isomer 5-oxo-Anion2 can undergo a cyclization to produce $CH_2C(O)OH$ anion $m/z = 59$.

Once generated, there are two different pathways for the isomer 5-oxo-Anion2 to follow:

- In pathway E1, the isomer 5-oxo-Anion2 has a carbonyl oxygen atom with a nucleophilic character. An intramolecular nucleophilic substitution can then take place (as illustrated in TS1 in Fig. 16) to eject an enolate anion of acetic acid $CH_2C(O)OH$.
- In pathway E2, the isomer 5-oxo-Anion2 can undergo a conformational change, through which the deprotonated acetyl group rotates 180° around a single internal C–C bond (see Fig. 16) to yield 5-oxo-Anion2-2 with a negligible energy barrier. Once formed, the CH_2 terminal of the deprotonated acetyl group can play the role of a nucleophile in this case. The nucleophilic methylene terminal can attack an internal carbon atom (as shown in TS3) to eject $CH_2C(O)OH$ anion with $m/z = 59$.

Although both pathways (E1 and E2) have nearly the same forward energy barrier, the reverse energy barrier in the case of pathway E2 is higher than that of pathway E1. This would favour the parent anion $[M-H]^-$ to follow pathway E2, especially due to higher stability of the ejected cyclobutanone ring (pathway E2) compared to 2-methylene oxetane neutral ring (pathway E1).

However, gas phase intramolecular nucleophilic substitution plays an important role in the fragmentation of the isomer 5-oxo-Anion2 $m/z = 129$. In both pathways, the same anion is formed. This anion was the first major fragment anion that could be detected as a result of the CID experiments even at low activation energy (10 eV).

3.4.4. Cyclization of 5-oxo-Anion3 isomer

Fig. 17 shows an energy profile, which produces the same anion $CH_2C(O)OH$ $m/z = 59$ discussed in Section 3.4.3.

Referring to Table 4, formation of isomer 5-oxo-Anion3 is by 4.5 kcal/mol energetically more favourable than formation of the isomer 5-oxo-Anion2. Despite this fact, the forward energy barrier for the nucleophilic gas phase intramolecular cyclization of 5-oxo-Anion3 is by at least 10 kcal/mol higher than that of 5-oxo-Anion2 isomer (compare Fig. 17 with Fig. 16).

Referring to experimental CID data shown in Fig. 12A, anion $m/z = 59$ could be seen even when a collision activation of just 10 eV was applied. If we assume, that 25% of the applied kinetic ion activation can be deposited as internal energy, 2.5 eV (57.6 kcal/mol) of internal energy is available for the pathway shown in Fig. 17 to be followed.

Figs. 16 and 17 show three different possibilities (with achievable forward energy barriers) for a parent anion $[M-H]^-$ $m/z = 129$ undergoing fragmentation to yield $CH_2C(O)OH^-$ $m/z = 59$. This explains why this fragment ion $m/z = 59$ is the most prominent one in the CID mass spectra shown in Fig. 12. In all three fragmentation pathways, which lead to ion $m/z = 59$, gas phase intramolecular nucleophilic substitution plays a key role.

3.4.5. H_2 elimination from $CH_2C(O)OH$ $m/z = 59$ anion. Is it possible?

We saw in previous Sections 3.4.3 and 3.4.4 that CH_2COOH anion $m/z = 59$ is formed as a result of a gas phase intramolecular nucleophilic substitution of one of the anionic isomers of 5-oxohexanoic acids (5-oxo-Anion2, 5-oxo-Anion2-2, 5-oxo-Anion3).

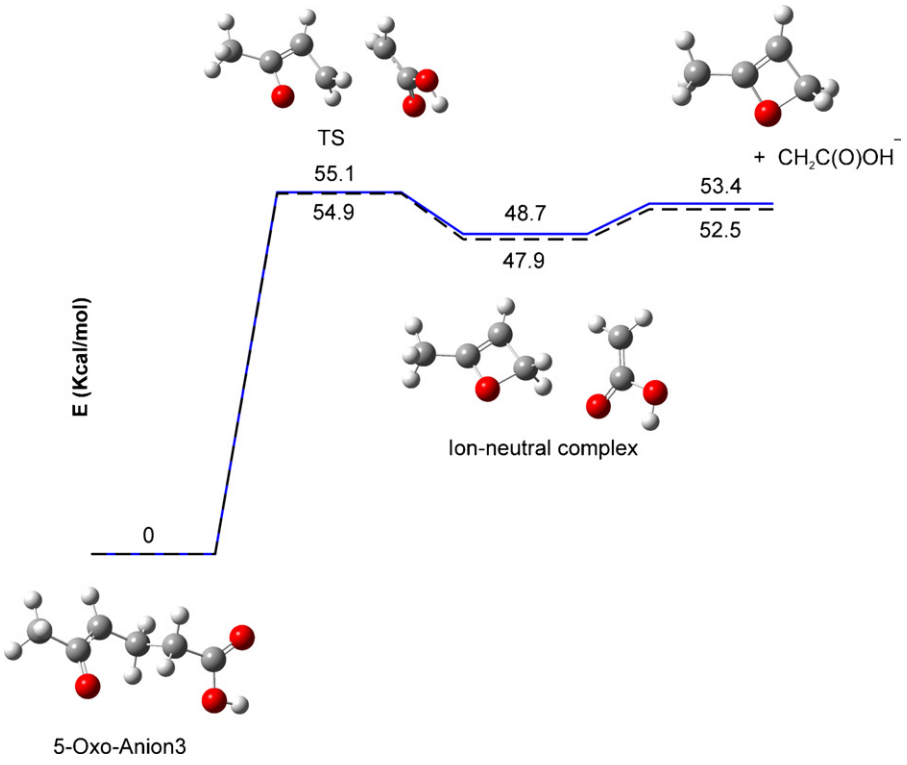

Fig. 17. Energy profile for the gas phase cyclization of isomer 5-oxo-Anion3 to yield anion CH_2=C(O)OH^- $m/z = 59$.

In this section we show that the fragment anion $m/z = 57$ formed in the CID mass spectra shown in Fig. 12B and C is not due to H_2 elimination from CH_2COOH anion, since the energy barrier for this event is too high (96.1 kcal/mol).

Even if we assume, that CH_2COOH anion can rearrange to generate CH_3COO^- anion through 1,3 H^+ shift (TS3 in Fig. 18), the energy barrier for H_2 elimination from acetate anion (65.3 kcal/mol) is higher than the energy barrier shown in Fig. 15 for acetonyl anion $CH_3C(O)CH_2^-$ $m/z = 57$ generation (41.2 kcal/mol).

Furthermore, H_2 elimination from acetate anion (65.3 kcal/mol) is thermodynamically less favourable compared with CH_2COOH anion generation through intramolecular nucleophilic substitution as seen in Fig. 16 above, which requires overcoming an energy barrier of 45.1 kcal/mol staring from 5-oxo-Anion2 isomer or 47.5 kcal/mol starting from 5-oxo-Anion2-2 isomer.

Thus, we are convinced that anion $m/z = 57$ is not generated by H_2 elimination from CH_2COOH anion or acetate anion. Anion $m/z = 57$ is formed through synchronous CO_2 and C_2H_4 elimination mechanism as shown in Fig. 15 and discussed in Section 3.4.2.

The theoretical mass difference between acetonyl anion $C_3H_5O^-$ and dehydrogenated acetate anion $C_2HO_2^-$ is 37 mDa. Thus, within a resolution of 2900 at nominal mass $m/z = 57$, signals representing these two anions must appear to generate a doublet, if both anions are formed. However, only one signal corresponding to the sum formula $C_3H_5O^-$ was observed upon collisional activation of $[M - H]^-$ of 5-oxohexanoic acid. This indicates that only the acetonyl anion is formed in the CID experiment.

3.4.6. A word about the minor fragment anion m/z = 71

The sum formula for the fragment ion $m/z = 71$, which is calculated based on accurate mass measurements in the CID spectra shown in Fig. 12, is $C_3H_3O_2^-$.

Ion $[M - H–H_2O]^-$ $m/z = 111$ generated from cone-voltage fragmentation of the parent anion $[M - H]^-$ $m/z = 129$ was further fragmented in the third quadrupole but no product ion $m/z = 71$ was observed. This indicates, that the fragment ion $m/z = 71$, which is observed in the CID mass spectra b and c in Fig. 12 must originate from the parent ion $[M - H]^-$ $m/z = 129$ itself. The accurate measured mass difference between the parent anion $m/z = 129$ and the fragment ion $m/z = 71$ represents the neutral sum formula C_3H_6O. No full DFT mechanism could be established for this minor ion formation. However, the proposed mechanism is shown in Scheme 1.

The geometry of the ion-neutral complex between acetonyl enolate ion and the neutral rest CH_2=CH–COOH (shown in Scheme 1) was optimized and is shown in Fig. 15 (after passing TS3 along pathway 2). If internal rotation of the neutral within the ion-neutral complex shown in Scheme 1 is feasible, the ion can abstract the carboxylic proton to generate an ion $m/z = 71$, since the carboxylic proton is the most acidic one in the neutral.

No transition state could be found to estimate the rotational barrier height. Ion and neutral rotational behaviour within ion-neutral complexes is well known in the literature [41,42]

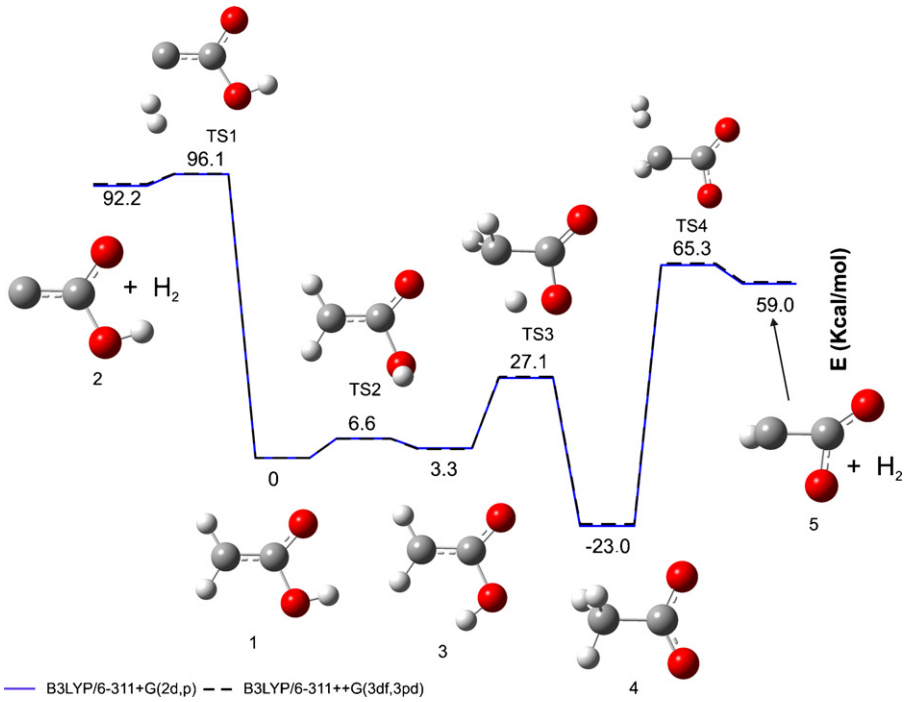

Fig. 18. Energy profile for H_2 elimination from CH_2COOH anion and acetate anion.

and reorientation behaviour could be discerned in positive ion-neutral complexes. The last reaction in Scheme 1, which represents deprotonation of the neutral CH_2=CH–COOH by the acetonyl anion within the ion-neutral complex, is exothermic $\Delta E^{298} = -12.7$ kcal/mol on B3LYP/6-311++G(3df,3pd) level of theory. Thus, this deprotonation can take place as a result of a gas phase ion-neutral reaction under thermal conditions without external energy supply, provided that this ion-neutral complex is previously generated from 5-oxo-Anion4 isomer ion. The forward energy barrier required to be overcome in order for the ion-neutral complex (shown in Scheme 1) to be formed is depicted in Fig. 15 (TS3 in pathway 2) and is equal to 31 kcal/mol (on the B3LYP/6-311++G(3df,3pd) level of theory).

4. Conclusion

Mass spectrometric characterization of two oxocarboxylic acids: 5-oxohexanoic acid and 6-oxoheptanoic acid in the negative ion mode was performed by the use of Q-TOF system coupled to an electrospray interface. Unusual fragmentation behaviour for the parent anions generated from these oxocarboxylic acids in comparison with their monocarboxylic acid analoga were discerned experimentally through CID experiments. In-depth analysis of the optimized anionic geometries, found transition states, and estimated energy barrier heights through density functional theory (DFT) allowed us to examine the mechanism of the various fragmentation channels of the parent anions. No CO_2 loss could be experimentally observed from $[M-H]^-$ of 5-oxohexanoic acid, while CO_2 ejection is partially inhibited from $[M-H]^-$ of 6-oxoheptanoic acid. Although water elimination was observed in both cases, ketene CH_2=C=O elimination followed by H_2 ejection was observed during fragmentation of the parent anion of 6-oxoheptanoic acid. Gas phase intramolecular nucleophilic substitution, by which fragment ion $m/z = 59$ was dominantly observed as a result of CID of the parent anion of 5-oxohexanoic acid, could be understood through DFT of its different parent anionic isomers. A difference in the internal carbon chain length between 5-oxohexanoic acid and 6-oxoheptanoic acid of just one carbon atom has a great influence on the fragmentation pattern of those analyzed acids.

Acknowledgements

Financial support by the Belgian Federal Public Planning Service Science Policy, Research Program “Science for a Sustainable Development” through Project IBOOT is gratefully acknowledged. B. Kanawati also thanks Prof. Dr. Jos Lelieveld for providing him with the instrumental facilities and Gaussian program required for carrying out this extensive study.

Appendix A. Supplementary data

Supplementary data associated with this article can be found, in the online version, at doi:10.1016/j.ijms.2007.07.014.

References

[1] K.F. Ho, S.C. Lee, J.J. Cao, K. Kawamura, T. Watanabe, Y. Cheng, J.C. Chow, Atmos. Environ. 40 (17) (2006) 3030.
[2] K. Kawamura, K. Yokoyama, Y. Fujii, O. Watanabe, J. Geophys. Res.-Atmos. 106 (D1) (2001) 1331.
[3] K. Kawamura, Anal. Chem. 65 (23) (1993) 3505.
[4] H.B. Wang, K. Kawamura, K. Yamazaki, J. Atmos. Chem. 53 (1) (2006) 43.

[5] A. Kubatova, R. Vermeylen, M. Claeys, J. Cafmeyer, W. Maenhaut, J. Geophys. Res.-Atmos. 107 (D21) (2002) (Art. No. 8343).
[6] G.H. Wang, S.L. Niu, C. Liu, L.S. Wang, Atmos. Environ. 36 (12) (2002) 1941.
[7] E.G. Stephanou, N. Stratigakis, Environ. Sci. Technol. 27 (7) (1993) 1403.
[8] A. Römpp, R. Winterhalter, G.K. Moortgat, Atmos. Environ. 40 (35) (2006) 6846.
[9] M. Glasius, M. Lahaniati, A. Calogirou, D. Di Bella, N.R. Jensen, J. Hjorth, D. Kotzias, B.R. Larsen, Environ. Sci. Technol. 34 (6) (2000) 1001.
[10] M. Jemal, O.Y. Zheng, D.S. Teitz, Rapid Commun. Mass Spectrom. 12 (8) (1998) 429.
[11] H.M. Liebich, G. Huesgen, A. Pickert, U. Stierle, J. Woll, J. High Resolut. Chromatogr. Chromatogr. Commun. 6 (9) (1983) 507.
[12] H. Budzikiewicz, Mass Spectrom. Rev. 5 (4) (1986) 345.
[13] J.H. Bowie, Mass Spectrom. Rev. 3 (2) (1984) 161.
[14] R. Isobe, I. Fujii, K. Kanematsu, Trac-Trends Anal. Chem. 6 (4) (1987) 78.
[15] N.B. Cech, C.G. Enke, Mass Spectrom. Rev. 20 (6) (2001) 362.
[16] R.B. Cole, Electrospray Ionization Mass Spectrometry. Part 1 – Chapter 1, John Wiley & Sons, Inc., 1997.
[17] B. Warscheid, T. Hoffmann, Rapid Commun. Mass Spectrom. 15 (23) (2001) 2259.
[18] J. Sunner, M.G. Ikonomou, P. Kebarle, Anal. Chem. 60 (13) (1988) 1308.
[19] J.S. Grossert, P.D. Fancy, R.L. White, Can. J. Chem.-Revue Canadienne De Chimie 83 (11) (2005) 1878.
[20] N.J. Jensen, G.W. Haas, M.L. Gross, Org. Mass Spectrom. 27 (4) (1992) 423.
[21] D.J. Mcadoo, Mass Spectrom. Rev. 7 (4) (1988) 363.
[22] P. Longevialle, Mass Spectrom. Rev. 11 (3) (1992) 157.
[23] C. Matthias, A. Cartoni, D. Kuck, Int. J. Mass Spectrom. 255 (2006) 195.
[24] A.J. Chalk, L. Radom, J. Am. Chem. Soc. 120 (33) (1998) 8430.
[25] Y.H. Song, H. Chen, R.G. Cooks, Rapid Commun. Mass Spectrom. 19 (23) (2005) 3493.
[26] J.A.A. Demmers, D.T.S. Rijkers, J. Haverkamp, J.A. Killian, A.J.R. Heck, J. Am. Chem. Soc. 124 (37) (2002) 11191.
[27] H. Lioe, R.A.J. O'Hair, G.E. Reid, J. Am. Soc. Mass Spectrom. 15 (1) (2004) 65.
[28] B.A. Collings, W.R. Stott, F.A. Londry, J. Am. Soc. Mass Spectrom. 14 (6) (2003) 622.
[29] T.J.D. Jorgensen, H. Gardsvoll, M. Ploug, P. Roepstorff, J. Am. Chem. Soc. 127 (8) (2005) 2785.
[30] M. Guilhaus, D. Selby, V. Mlynski, Mass Spectrom. Rev. 19 (2) (2000) 65.
[31] M.J. Frisch, G.W. Trucks, H.B. Schlegel, G.E. Scuseria, M.A. Robb, J.R. Cheeseman, J.A. Montgomery Jr., T. Vreven, K.N. Kudin, J.C. Burant, J.M. Millam, S.S. Iyengar, J. Tomasi, V. Barone, B. Mennucci, M. Cossi, G. Scalmani, N. Rega, G.A. Petersson, H. Nakatsuji, M. Hada, M. Ehara, K. Toyota, R. Fukuda, J. Hasegawa, M. Ishida, T. Nakajima, Y. Honda, O. Kitao, H. Nakai, M. Klene, X. Li, J.E. Knox, H.P. Hratchian, J.B. Cross, V. Bakken, C. Adamo, J. Jaramillo, R. Gomperts, R.E. Stratmann, O. Yazyev, A.J. Austin, R. Cammi, C. Pomelli, J.W. Ochterski, P.Y. Ayala, K. Morokuma, G.A. Voth, P. Salvador, J.J. Dannenberg, V.G. Zakrzewski, S. Dapprich, A.D. Daniels, M.C. Strain, O. Farkas, D.K. Malick, A.D. Rabuck, K. Raghavachari, J.B. Foresman, J.V. Ortiz, Q. Cui, A.G. Baboul, S. Clifford, J. Cioslowski, B.B. Stefanov, G. Liu, A. Liashenko, P. Piskorz, I. Komaromi, R.L. Martin, D.J. Fox, T. Keith, M.A. Al-Laham, C.Y. Peng, A. Nanayakkara, M. Challacombe, P.M.W. Gill, B. Johnson, W. Chen, M.W. Wong, C. Gonzalez, J.A. Pople, Gaussian 03, Revision D, Gaussian, Inc., Wallingford, CT, 2004.
[32] H.B. Schlegel, J. Comput. Chem. 3 (2) (1982) 214.
[33] P. Csaszar, P. Pulay, J. Molec. Struct. 114 (1984) 31.
[34] O. Farkas, H.B. Schlegel, Phys. Chem. Chem. Phys. 4 (1) (2002) 11.
[35] O. Farkas, H.B. Schlegel, J. Chem. Phys. 111 (24) (1999) 10806.
[36] C. Gonzalez, H.B. Schlegel, J. Chem. Phys. 90 (4) (1989) 2154.
[37] D.K. Malick, G.A. Petersson, J.A. Montgomery, J. Chem. Phys. 108 (14) (1998) 5704.
[38] C. Gonzalez, H.B. Schlegel, J. Phys. Chem. 94 (14) (1990) 5523.
[39] R. Dennington II, T. Keith, J. Millam, K. Eppinnett, W.L. Hovell, R. Gilliland, GaussView, Version 3.0.9, Semichem, Inc., Shawnee Mission, KS, 2003.
[40] R.B. Cole, Electrospray Ionization Mass Spectrometry, Chapter 12, Section IV-C, John Wiley & Sons, Inc., 1997.
[41] J.C. Traeger, T.H. Morton, J. Am. Soc. Mass Spectrom. 15 (7) (2004) 989.
[42] T.H. Morton, Org. Mass Spectrom. 27 (1992) 353.